

Article

Zintl Salts $\text{Ba}_2\text{P}_7\text{X}$ ($\text{X} = \text{Cl}, \text{Br}, \text{and I}$): Synthesis, Crystal, and Electronic Structures

Juli-Anna Dolyniuk and Kirill Kovnir *

Department of Chemistry, University of California, Davis, One Shields Avenue, Davis, CA 95616, USA; E-Mail: jdolyniuk@ucdavis.edu

* Author to whom correspondence should be addressed; E-Mail: kkovnir@ucdavis.edu;
Tel.: +1-530-752-5563; Fax: +1-530-752-8995.

Received: 1 June 2013; in revised form: 16 July 2013 / Accepted: 6 August 2013 /

Published: 26 August 2013

Abstract: Two barium phosphide halides, $\text{Ba}_2\text{P}_7\text{Br}$ and $\text{Ba}_2\text{P}_7\text{I}$, were synthesized and structurally characterized by single crystal X-ray diffraction. Both compounds crystallize in the monoclinic space group $P2_1/m$ (No. 11) and are isostructural to $\text{Ba}_2\text{P}_7\text{Cl}$. The crystal structures of $\text{Ba}_2\text{P}_7\text{X}$ ($\text{X} = \text{Cl}, \text{Br}, \text{I}$) feature the presence of heptaphosphanortricyclane P_7^{3-} clusters along with halogen anions and barium cations. According to the Zintl concept, $\text{Ba}_2\text{P}_7\text{X}$ compounds are electron-balanced semiconductors. Quantum-chemical calculations together with UV-Visible spectroscopy confirm the title compounds are wide bandgap semiconductors. The bonding in the P_7^{3-} clusters was analyzed by means of electron localization function. The elemental compositions were confirmed using energy dispersive X-ray spectroscopy.

Keywords: Zintl phase; crystal structure; P_7 cluster; heptaphosphanortricyclane; electronic structure; electron localization function

1. Introduction

Polyphosphides are known to form a variety of crystal structures with different elements [1–15]. From three-dimensional frameworks to isolated cages, phosphorous backbones form a wide range of stable structures. The P_7^{3-} cluster, heptaphosphanortricyclane, heptaphosphatricyclo[2.2.1.0(2,6)]heptane, is a commonly present phosphorus fragment which is able to form binary and ternary compounds with different counter-cations, like A_3P_7 ($\text{A} = \text{alkali metal}$) or Ba_3P_{14} [1–5]. The P_7^{3-} clusters are quite stable

and have been found in both solution and solid phases [1–5,15]. Heavier analogs of such clusters with As and Sb are also known [16–18].

Similar to other intermetallics, the electronic structures of polyphosphides can be rationalized by application of the Zintl concept [19,20]. Zintl theory implies the valence electrons of electropositive atoms are donated to more electronegative atoms. The latter realize their electron octet by forming $2c-2e$ chemical bonds and by having electron lone pairs. In A_3P_7 , one electron is donated from each A atom to allow for the formation of the P_7^{3-} cage [4]. In Ba_3P_{14} , three Ba atoms donate two electrons each to allow for the formation of two P_7^{3-} cages [3]. An interesting example of a compound combining the P_7^{3-} Zintl anion with a classical chloride anion was reported by von Schnering and Menge in 1981 [21]. In the Ba_2P_7Cl Zintl salt, the total charge of two Ba^{2+} cations is compensated by a combination of Cl^- and P_7^{3-} anions. In this work, we expand the family of P_7^{3-} structures to include the isostructural Ba_2P_7Br and Ba_2P_7I . We report the synthesis, characterization, and chemical bonding of three Ba_2P_7X ($X = Cl, Br, I$) compounds.

2. Results and Discussion

2.1. Crystal Structure

Originally, Ba_2P_7I was discovered accidentally during attempts to grow large single crystals of BaP_3 utilizing I_2 as a transport reagent. After the crystal structure and composition were established, a sample of Ba_2P_7I was synthesized by the reaction of stoichiometric amounts of the elements at 1073 K. The bromine-containing analog was synthesized from barium, red phosphorus, and barium bromide at the same temperature. A summary of pertinent information related to single crystal X-ray diffraction unit cell parameters, data collection, and refinements is provided in Table 1. Energy-dispersive X-ray spectroscopy (EDS) investigations of the selected single crystals confirmed the presence of only the expected Ba, P, and X halogen elements.

Table 1. Data collection and structure refinement parameters for Ba_2P_7X ($X = Cl, Br, I$). *

Composition	Ba_2P_7Cl	Ba_2P_7Br	Ba_2P_7I
CSD number	426193	426194	426195
Space Group		$P2_1/m$ (No. 11)	
Temperature [K]		90(2)	
λ [Å]		Mo K_{α} , 0.71073	
a [Å]	6.329(1)	6.294(1)	6.3538(3)
b [Å]	6.805(1)	6.835(1)	6.8990(4)
c [Å]	11.709(2)	11.850(2)	12.0392(6)
β [deg]	95.267(2)	95.819(2)	95.915(1)
V [Å ³]	502.2(1)	507.2(2)	524.93(5)
Z		2	
ρ [g cm ⁻³]	3.485	3.742	3.912
μ [mm ⁻¹]	9.099	12.686	11.392
θ [deg.]	$3.23 < \theta < 30.66$	$3.25 < \theta < 30.57$	$3.22 < \theta < 30.58$
data/parameters	1671/55	1671/55	1733/55
R_1 ($I > 2\sigma(I)$)	0.028	0.012	0.019

Table 1. Cont.

Composition	Ba ₂ P ₇ Cl	Ba ₂ P ₇ Br	Ba ₂ P ₇ I
wR ₂ (I > 2σ(I))	0.047	0.025	0.037
Goodness-of-fit	1.087	1.202	1.117
Δρ _{max} and Δρ _{min} , e/Å ³	1.36 and −1.14	0.50 and −0.73	1.22 and −0.92

* More information can be obtained from Fachinformations-Zentrum Karlsruhe, D-76344 Eggenstein-Leopoldshafen, Germany, by quoting the depository CSD (Crystal Structure Database) numbers given above.

The new compounds, Ba₂P₇Br and Ba₂P₇I, are isostructural to the previously reported Ba₂P₇Cl (Figure 1) [21]. The crystal structure of Ba₂P₇X can be described as consisting of two distinct ionic layers, [Ba₂X₂]²⁺ and [Ba₂(P₇)₂]^{2−} stacked along the [001] direction (Figure 2a). According to the Zintl concept [19,20], the Ba₂P₇X compounds are electron balanced. The barium and halogen atoms realize their electron octet by donating and accepting two and one electrons, respectively. Phosphorous atoms bonded to three other phosphorus atoms should be P⁰, realizing their electron octet by maintaining an electron lone pair. Phosphorous atoms bonded to two other phosphorus atoms should be P^{1−}, realizing their electron octet by maintaining two electron lone pairs. The P₇^{3−} clusters contain four three-bonded phosphorus atoms (P1, P2, P5) and three two-bonded P atoms (P3, P4) (Figure 3a). Thus, the total charge per cluster is −3, (3b-P⁰)₄(2b-P^{1−})₃, and the charge-balanced formula is (Ba²⁺)₂(P₇^{3−})(X[−]). In accordance with this formulation, the halogen atoms of Ba₂P₇X are surrounded by barium atoms in the first coordination sphere, while the phosphorus atoms are situated further apart. The P₇^{3−} units are surrounded by barium atoms coordinating to the faces, edges, and corners of the cluster (Figure 3b). The Ba–P separations for all Ba₂P₇X are in the range of 3.3–3.6 Å. The shortest P–X interatomic separations are longer than 3.6 Å.

Figure 1. Crystal structure of Ba₂P₇X (X = Cl, Br, I) projected along the (a) [100] and (b) [010] directions. Ba: red; P: brown; X: green. The shortest Ba–X distance is indicated with a dashed line.

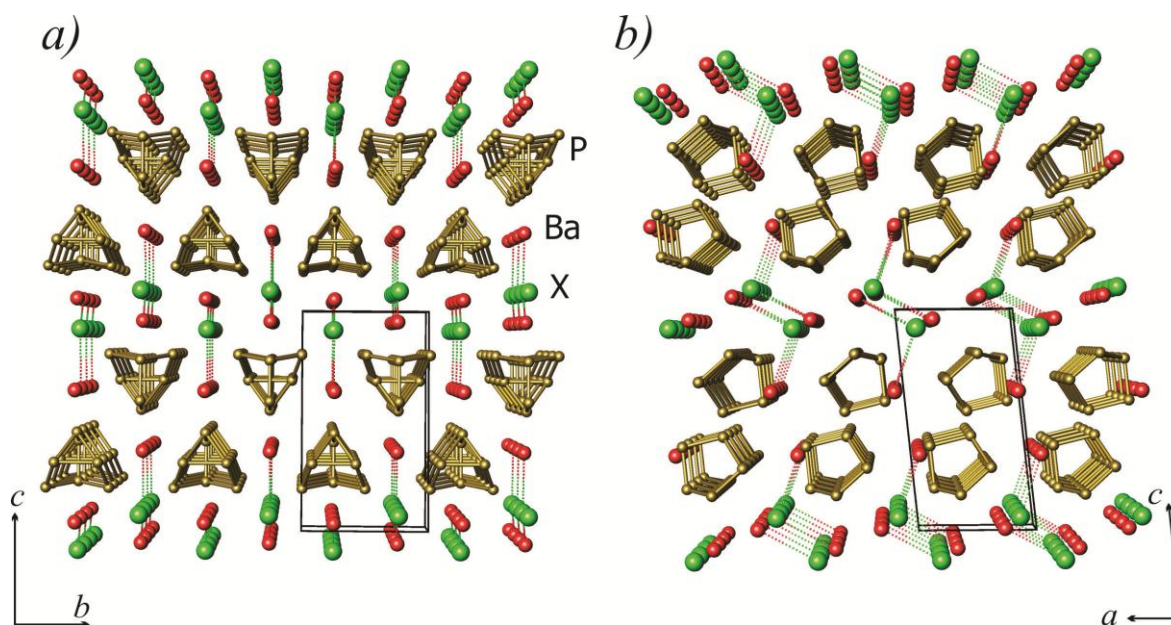


Figure 2. Comparison of the P_7^{3-} heptaphosphanortricyclane clusters arrangements in the crystal structures of (a) Ba_2P_7X and (b) Ba_3P_{14} [3]. Barium atoms are shown in red; halogen atoms in green; and phosphorous clusters in blue.

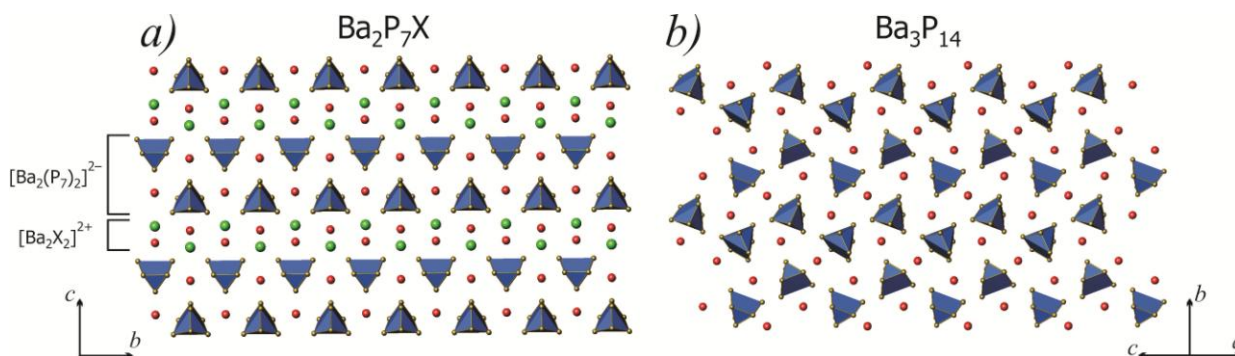
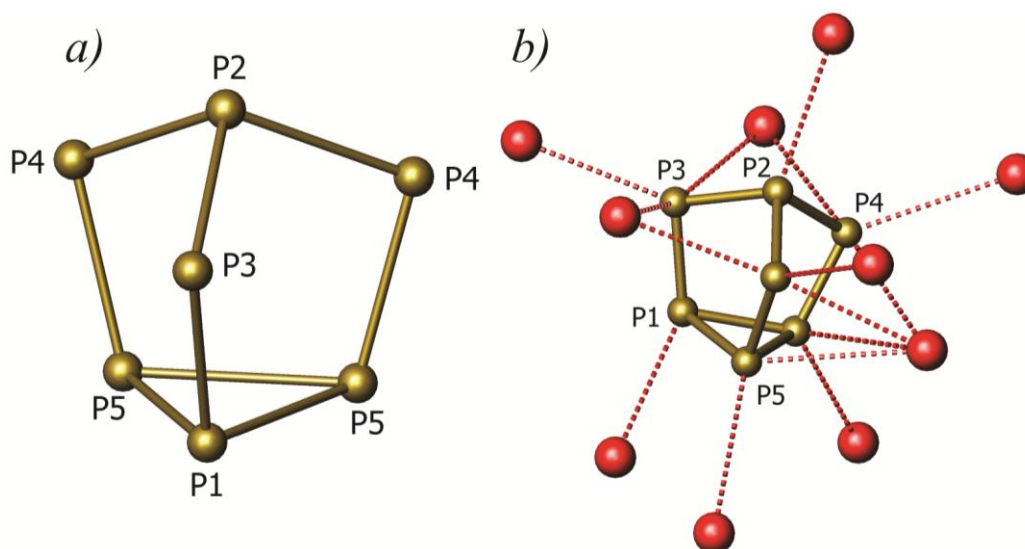


Figure 3. (a) The structure of the heptaphosphanortricyclane (P_7) $^{3-}$ cluster and (b) its coordination by barium atoms in the crystal structures of Ba_2P_7X ($X = Cl, Br, I$).



An interesting feature of the Ba_2P_7X crystal structure is the relative arrangement of its P_7^{3-} fragments. All fragments are arranged parallel to each other in a head-to-head fashion. To the best of our knowledge, no other structures composed of the P_7^{3-} anions are known to form with such straight linear arrangements of P_7^{3-} anions. For example, in Ba_3P_{14} , the heptaphosphanortricyclane clusters are rotated with respect to each other (Figure 2b) [3]. Apparently, the presence of $[Ba_2X_2]^{2+}$ layers fixes the orientation of the P_7^{3-} clusters, probably due to the repulsion between negatively charged species. The lack of halogen atoms in Ba_3P_{14} allows for more structural flexibility, and the P_7^{3-} clusters are free to face different directions.

In Ba_2P_7X , the P_7^{3-} cluster is made up of only five symmetrically unique phosphorous atoms. Bond lengths and angles, and a general view of the P_7^{3-} clusters are presented in Table 2 and Figure 3, respectively. The heptaphosphanortricyclane of Ba_2P_7X has C_s local symmetry with a mirror plane containing the P1, P2, and P3 atoms. In Ba_3P_{14} , A_3M_7 ($A = \text{alkali metal}$), and ammonia solvates of alkali metal phosphides, the P_7^{3-} heptaphosphanortricyclane clusters have C_1 local symmetry [3,4,15].

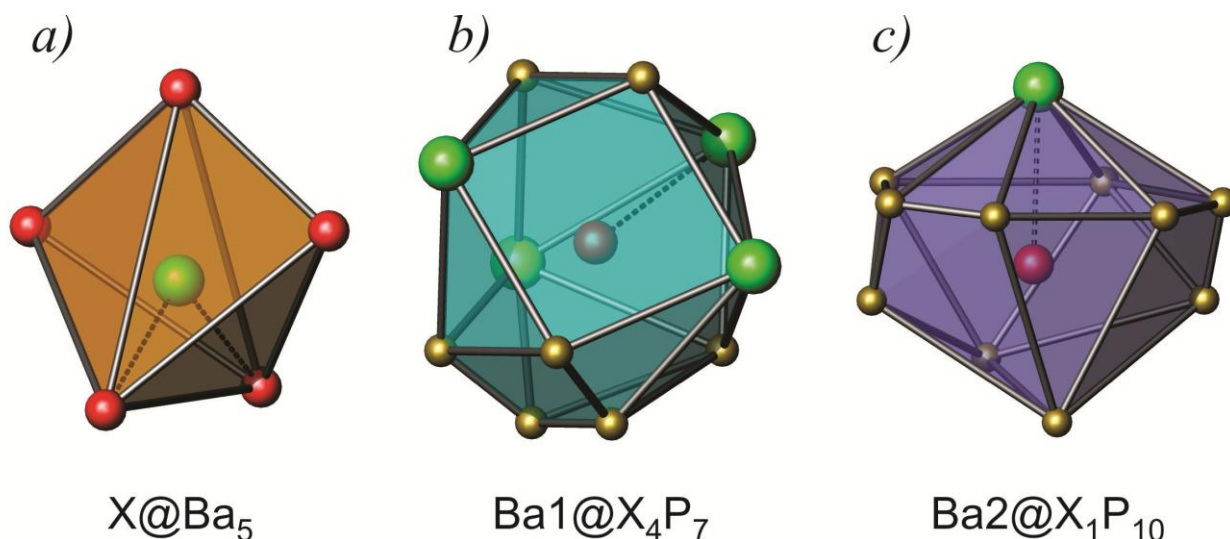
Table 2. P–P bond distances and angles in the crystal structures of Ba₂P₇X (X = Cl, Br, I).

Atoms	Distances (Å)			Angle Type	Angle (θ)		
	Ba ₂ P ₇ Cl	Ba ₂ P ₇ Br	Ba ₂ P ₇ I		Ba ₂ P ₇ Cl	Ba ₂ P ₇ Br	Ba ₂ P ₇ I
P1–P3	2.156(2)	2.1558(9)	2.156(1)	∠P1–P3–P2	97.51(8)	97.65(3)	97.77(6)
P1–P5	2.229(2)	2.2307(7)	2.233(1)	∠P2–P4–P5	99.53(7)	99.53(3)	99.47(4)
P2–P3	2.188(2)	2.1853(9)	2.188(1)	∠P1–P5–P4	105.44(7)	105.23(3)	104.88(5)
P2–P4	2.170(1)	2.1706(6)	2.180(1)	∠P1–P5–P5	58.26(4)	58.38(1)	58.41(2)
P4–P5	2.143(2)	2.1434(6)	2.154(1)	∠P5–P1–P5	63.49(7)	63.24(3)	63.19(5)
P5–P5	2.345(2)	2.339(1)	2.340(2)	–	–	–	–

The P₇^{3−} clusters of Ba₂P₇X contain phosphorus atoms P1 and P5 in strained geometries, with angles in the basal triangle close to 60°. Other angles are significantly larger and closer to the typical tetrahedral angles found in most polyphosphide anions. In the P₇^{3−} clusters of Ba₃P₁₄ and Li₃P₇, the P–P distances in the basal triangle are similar, 2.23–2.29 Å [3,4]. In Ba₂P₇X, the P–P bond perpendicular to the mirror plane is significantly elongated compared to the other two basal triangle bonds: $d(\text{P5–P5}) = 2.34$ Å, $d(\text{P1–P5}) = 2.23$ Å. The other bond lengths and angles in the Ba₂P₇X P₇^{3−} clusters appear to be similar to those found in the crystal structures of Ba₃P₁₄ and Li₃P₇.

The local coordination of the barium and halogen atoms is shown in Figure 4. Five barium atoms form the first coordination sphere of the halogen atoms. Each barium atom is surrounded by 11 neighbors. Four halogen atoms and seven phosphorus atoms form irregular polyhedra around Ba1, while the Ba2 atoms are surrounded by 10 phosphorus atoms and only one halogen atom. As expected, with an increase of the halogen size from chlorine to iodine, the unit cell volume increases (Table 1). The P₇^{3−} unit remains nearly the same in all three Ba₂P₇X compounds (Table 2). The shortest Ba–P distance also exhibits a minor variation upon a change in the halogen atom, with the shortest Ba2–P distance remaining the same in all compounds: 3.30–3.31 Å. An increase of the unit cell occurs mainly due to the increase in the shortest Ba–X distances from 3.14 Å (Cl) to 3.32 Å (Br) to 3.47 Å (I).

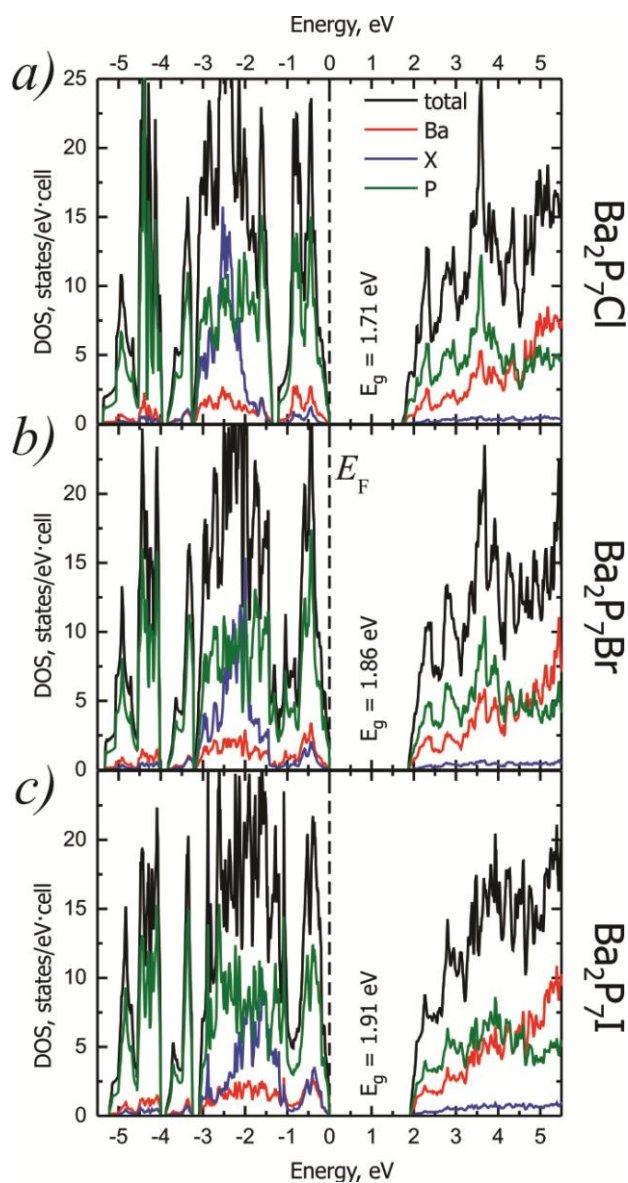
Figure 4. The local coordination of (a) halogen atoms and (b,c) barium atoms in Ba₂P₇X. The shortest Ba–X distance is indicated with dashed lines.



2.2. Electronic Structure

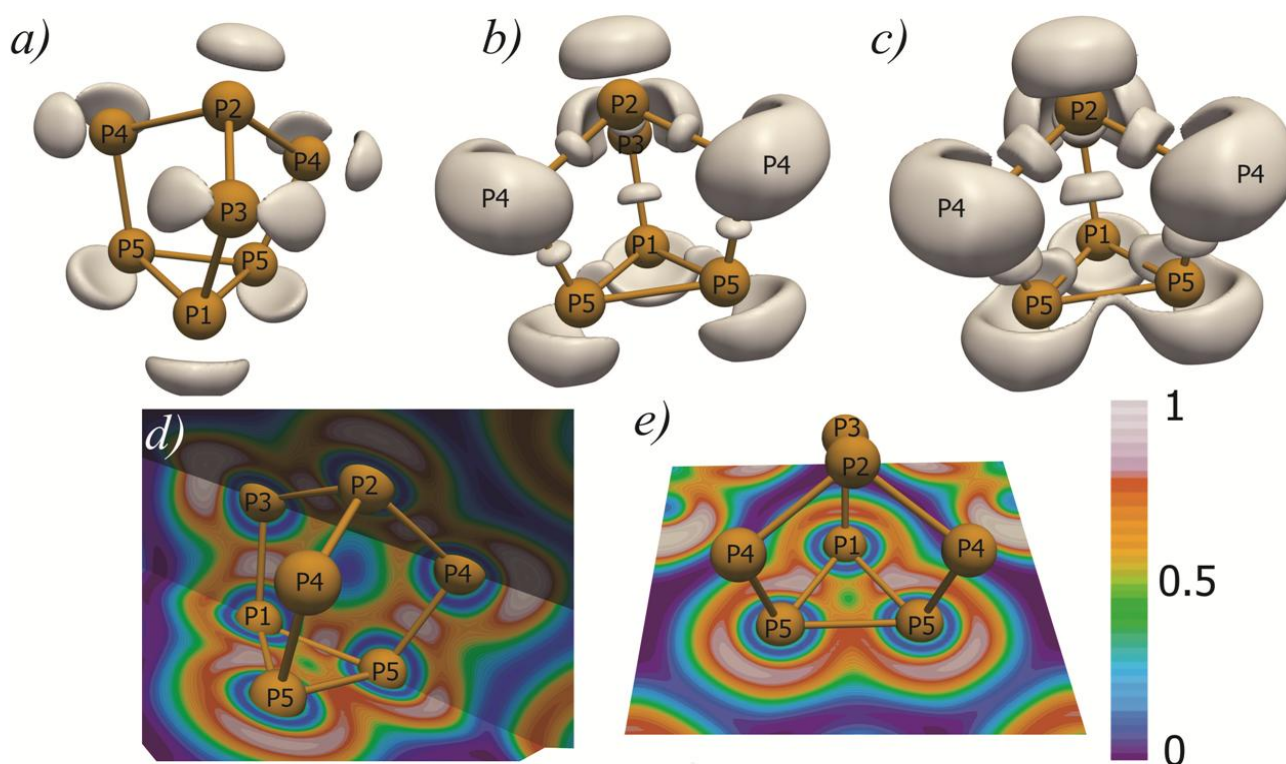
The electron balanced Zintl salts, $\text{Ba}_2\text{P}_7\text{X}$, are expected to exhibit semiconducting and diamagnetic properties. Band structure calculations were performed to verify this description (Figure 5). According to the calculations, the $\text{Ba}_2\text{P}_7\text{X}$ compounds are wide band-gap semiconductors with indirect bandgaps $E_g = 1.71$ eV ($\text{X} = \text{Cl}$), 1.86 eV ($\text{X} = \text{Br}$), 1.91 eV ($\text{X} = \text{I}$). The results of calculations were verified with UV-Vis spectroscopy (*vide infra*). In the electronic structure of $\text{Ba}_2\text{P}_7\text{X}$, the top of the valence band is dominated by the contribution of phosphorus 3p orbitals, with both halogen and barium orbitals also contributing to the states near the Fermi level. The contribution of the halogen orbitals to the states near the Fermi level increases in the Cl–Br–I series. The bottom of the conduction band is comprised of phosphorus and barium orbitals with negligible contributions from halogen orbitals. The main contribution of halogen p-orbitals to the valence band is located between -1 and -3 eV.

Figure 5. Density of states (DOS) diagram for $\text{Ba}_2\text{P}_7\text{X}$, (a) $\text{X} = \text{Cl}$; (b) $\text{X} = \text{Br}$; and (c) $\text{X} = \text{I}$. Contributions from Ba, P, and X orbitals are shown in red, green, and blue colors, respectively.



To clarify the bonding in the P_7^{3-} phosphorus clusters, we applied Electron Localization Function (ELF) analysis [22–25] to the Ba_2P_7I compound (Figure 6). According to the Zintl concept, single covalent $2e-2c$ bonds are expected to be present at short P–P interatomic separations. Additionally, one and two electron lone pairs are expected to be located on the two- and three-bonded phosphorus atoms, respectively. The ELF analysis indicates the presence of the expected number of electron lone pairs (Figure 6a). The two bonded phosphorus atoms, P4 and P3, have two electron lone pairs, while the three-bonded P1, P2, and P5 have only one electron lone pair. These results are similar to the results of ELF calculations for less symmetric P_7^{3-} clusters [15].

Figure 6. Top: 3D isosurfaces of electron localization function (η) for the P_7^{3-} phosphorus cluster in Ba_2P_7I , (a) $\eta = 0.91$; (b) $\eta = 0.83$; (c) $\eta = 0.765$. Bottom: coloring of the electron localization function distribution for the slices of the phosphorus cluster in Ba_2P_7I (d,e). The color bar is given in the right bottom corner.



Localization domains corresponding to the covalent two centered P–P interactions were found for all of the short interatomic separations (Figure 6b–e). The ELF maxima of the P1–P5 bonds were shifted from the lines connecting the P1 and P5 atoms. The ELF domain for the P5–P5 bond exhibited lower values of ELF (Figure 6c). This localization domain is also shifted from the line connecting the P5 atoms and it is not well separated from the domains corresponding to the electron lone pairs on the P5 atoms (Figure 6c–e). The P1–P5–P5 basal triangle, with a topology close to that of cyclopropane, is the most strained face of the P_7^{3-} cluster. Angles of $\sim 60^\circ$ hamper the direct overlap of phosphorus orbitals. This explains the displacement of the bonding maxima from the lines connecting the atoms.

In ELF studies performed for the P_7^{3-} clusters of the ammonia solvates of alkali metal phosphides, the heptaphosphanortricyclane units are less symmetric, with point group C_1 [15]. These units have

almost identical bonds, 2.26–2.30 Å, between phosphorus atoms forming a strained basal triangle. Three well-separated and similar localization domains were found displaced from the line connecting phosphorus atoms [15]. Heptaphosphanortricyclane units in $\text{Ba}_2\text{P}_7\text{X}$ have a different geometry (Table 2) with shorter P1–P5 distances (2.23 Å) and longer P5–P5 distance (2.34 Å) than those distances present in ammonia solvate compounds [15]. This difference is probably due to the presence of a Ba atom coordinated to the P4–P5–P5–P4 square (Figure 3b) [21]. This is reflected in the bonding picture: the localization domains for P1–P5 bonds are well pronounced and remain separated from the lone pair domains, while the localization domain for the P5–P5 bond is less pronounced and is not separated from the domains corresponding to the lone pairs located on the P5 atoms (Figure 6e).

No ELF maxima were detected near the shortest Ba–X separations, which are indicated by the dashed lines in Figures 1 and 4. Presumably, all Ba–X interactions are electrostatic cation-anion interactions.

2.3. UV-Vis Spectroscopy

$\text{Ba}_2\text{P}_7\text{Cl}$, $\text{Ba}_2\text{P}_7\text{Br}$, and $\text{Ba}_2\text{P}_7\text{I}$ are red, orange, and yellow-orange, respectively. Solid state UV-Visible spectroscopy was employed for experimental bandgap determinations.

According to the calculated Tauc plots [26,27], $\text{Ba}_2\text{P}_7\text{Cl}$ has indirect optical transitions corresponding to a bandgap of 1.83(2) eV (Figure 7, Table 3). The calculated bandgap for this compound, 1.71 eV, is in reasonable agreement with the experimental data. Calculations predict the increase of the bandgaps in the Cl–Br–I series (Figure 5). This increase was observed experimentally and is consistent with the visual color change of the $\text{Ba}_2\text{P}_7\text{X}$ analogs from red to yellow. The experimental indirect bandgaps of the bromine and iodine analogs, 1.92(4) eV and 1.89(2) eV, respectively, are approximately 0.1 eV larger than the $\text{Ba}_2\text{P}_7\text{Cl}$ bandgap. In our UV-Vis experiments we were not able to detect the small predicted difference between the indirect bandgap values for $\text{Ba}_2\text{P}_7\text{Br}$ and $\text{Ba}_2\text{P}_7\text{I}$, when estimated standard deviations are taken into account. A combination of the spectroscopic and calculation approaches indicates the compounds obtained are wide bandgap semiconductors.

Figure 7. Solid-state UV-Visible spectra of $\text{Ba}_2\text{P}_7\text{X}$ (X = Cl, Br, I) compounds. (a) Kubelka-Munk diffuse reflectance; (b) and (c) Tauc plots for allowed direct and indirect transitions, respectively.

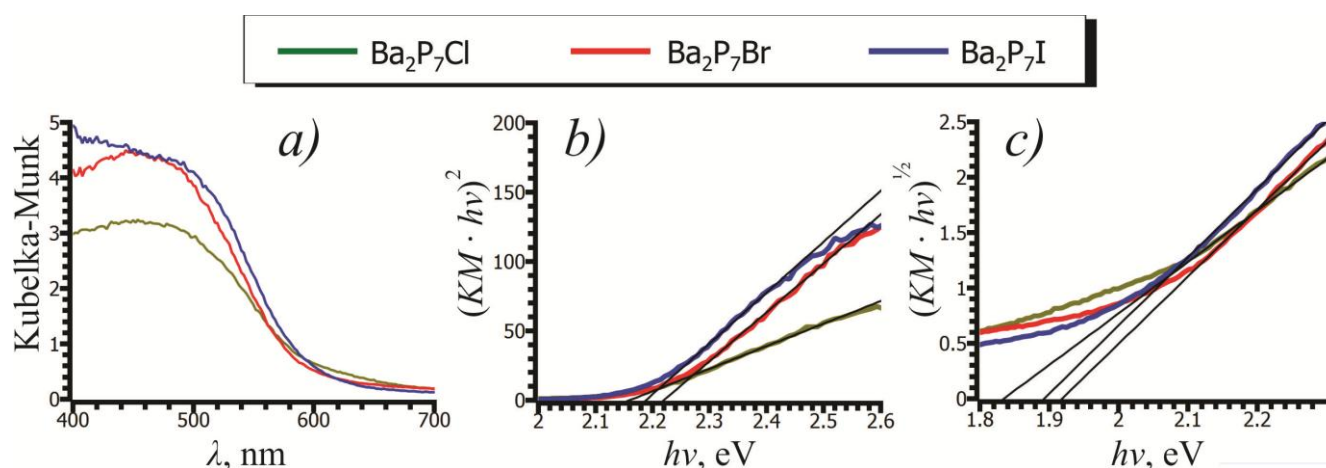


Table 3. Experimental and calculated values for the Ba₂P₇X bandgaps.

Composition	Ba ₂ P ₇ Cl	Ba ₂ P ₇ Br	Ba ₂ P ₇ I
Direct Bandgap (eV)	2.16(3)	2.20(4)	2.19(4)
Indirect Bandgap (eV)	1.83(2)	1.92(2)	1.89(2)
Calculated Bandgap (eV)	1.71	1.86	1.91

3. Experimental Section

All samples of Ba₂P₇Cl, Ba₂P₇Br, and Ba₂P₇I were prepared via solid-state reactions in evacuated and sealed silica ampoules. The samples were prepared in an Argon-filled glovebox with $p(\text{O}_2)$ and $p(\text{H}_2\text{O}) < 1$ ppm. The starting materials: metallic barium (Sigma Aldrich, St. Louis, MO, USA, 99.9%), iodine (Alfa Aesar, Ward Hill, MA, USA, 99.9985%), and red phosphorous (Alfa Aesar, Ward Hill, MA, USA, 99%) were used as received. Barium bromide and barium chloride (Alfa Aesar, Ward Hill, MA, USA, 99.998% and 99%, respectively) were heated at 573 K overnight under an inert atmosphere to remove traces of water.

A single phase sample of Ba₂P₇I was synthesized by annealing stoichiometric amounts of the elements at 1073 K for 140 h. Samples of Ba₂P₇Cl and Ba₂P₇Br were prepared using metallic barium, phosphorous, and barium chloride or barium bromide in a 3:14:1 ratio under similar annealing conditions. In agreement with the previous report [21], Ba₂P₇Cl crystals have a red color. Ba₂P₇Br and Ba₂P₇I crystals exhibit orange and orange-yellow colors, respectively. The color of all Ba₂P₇X lightened upon grinding. Similar to other compounds containing the P₇³⁻ phosphorus cluster, Ba₂P₇X degrades in air over time, and appears to quickly decompose in water, so samples were stored in an Argon-filled glovebox.

The samples were characterized by X-ray powder diffraction (XRD) using a Bruker D8 Advance diffractometer employing Cu K_α radiation. Elemental analysis of the selected single crystals was carried out on a Hitachi S4100T scanning electron microscope (SEM) with energy-dispersive X-ray (EDX) microanalysis (Oxford INCA energy). Sample analysis confirmed the presence of only Ba, P, and X (X = Cl, Br, I). Solid-state UV-Visible spectroscopy (Thermo Scientific Evolution 220 Spectrometer) was employed for experimental bandgap determinations. For UV-Vis measurements, solid samples were ground into powders and gently pressed onto rough filter paper to form a thick layer of sample. Attempts to dissolve samples of Ba₂P₇X for solution-based UV-Vis measurements were unsuccessful. Samples of Ba₂P₇X were water sensitive, turning to amorphous yellow material when immersed. No visible color change was observed for immersion in ethanol, but as samples dried they turned brown.

Single crystal X-ray diffraction experiments were carried out at 90 K using a Bruker AXS SMART diffractometer with an APEX-II CCD detector and Mo K_α radiation. The data sets were recorded as ω -scans at a 0.3° stepwidth and integrated with the Bruker SAINT software package [28]. A multiscan absorption correction was applied. The solution and refinement of crystal structures were carried out using the SHELX suite of programs [29]. The structures were solved in the $P2_1/m$ space group and the final refinement was performed using anisotropic atomic displacement parameters for all atoms.

Density functional band structure calculations and bonding analyses were carried out using the tight binding—linear muffin tin orbitals—atomic sphere approximation (TB-LMTO-ASA) program

package [30]. The Barth–Hedin exchange potential was employed for the local density approximation (LDA) calculations [31]. The radial scalar-relativistic Dirac equation was solved to obtain partial waves. A basis set containing Ba(6s,5d,4f), P(3s,3p), Cl(3p), Br(4p), and I(5p) orbitals was employed for a self-consistent calculation, with Ba(6p), P(3d), Cl(4s,3d), Br(5s,4d), and I(6s,5d,4f) functions being downfolded. The ELF (η) was evaluated with modules implemented within the TB–LMTO–ASA program package [22–24]. The ParaView program was used for visualization of ELF isosurfaces [32,33].

4. Conclusions

Two new compounds, Ba₂P₇Br and Ba₂P₇I, have been synthesized and their crystal structures have been determined by means of single crystal X-ray diffraction. In the crystal structure of Ba₂P₇X (X = Cl, Br, I) negatively charged layers of heptaphosphanortricyclane P₇³⁻ clusters surrounded by barium cations are stacked along the [001] direction, alternating with positively charged Ba₂X₂ layers. According to the Zintl count and quantum-chemical calculations, Ba₂P₇X are electron-balanced semiconductors with wide bandgaps. UV-Vis spectroscopy confirms the semiconducting nature of Ba₂P₇X compounds. Analysis of the chemical bonding in P₇³⁻ clusters by means of electron localization function indicates their bonding generally follows the Zintl counting scheme. However, for the basal triangle of phosphorus atoms, the ELF localization domains are displaced from the shortest interatomic separations.

Acknowledgments

The authors would like to thank J. Zhao and J. Wang for their assistance with the UV-Vis measurements. This research is supported by the U.S. Department of Energy, Office of Basic Energy Sciences, Division of Materials Sciences and Engineering under Award DE-SC0008931.

Conflicts of Interest

The authors declare no conflict of interest.

References

1. Pöttgen, R.; Höhle, W.; von Schnering, H.G. Phosphides: Solid State Chemistry. In *Encyclopedia of Inorganic Chemistry*, 2nd ed.; King, R.B., Ed.; Wiley: Chichester, UK, 2005; volume 8, pp. 4255–4308.
2. Von Schnering, H.G.; Hoenle, W. Bridging chasms with polyphosphides. *Chem. Rev.* **1988**, *88*, 243–273.
3. Dahlmann, W.; von Schnering, H.G. Die Polyphosphide SrP₃ und Ba₃P₁₄. *Naturwissenschaften* **1973**, *60*, 429–429.
4. Manriquez, V.; Höhle, W.; von Schnering, H.G. Trilithiumheptaphosphid Li₃P₇: Darstellung, Struktur und Eigenschaften. *Z. Anorg. Allg. Chem.* **1986**, *539*, 95–109.

- Scharfe, S.; Kraus, F.; Stegmaier, S.; Schier, A.; Fäsler, T.F. Zintl ions, cage compounds, and intermetalloid clusters of group 14 and group 15 elements. *Angew. Chem. Int. Ed.* **2011**, *50*, 3630–3670.
- Shatruck, M.M.; Kovnir, K.A.; Shevelkov, A.V.; Popovkin, B.A. Ag_3SnP_7 : A polyphosphide with a unique (P_7) chain and a novel Ag_3Sn heterocluster. *Angew. Chem. Int. Ed.* **2000**, *39*, 2508–2509.
- Lange, S.; Sebastian, C.P.; Zhang, L.; Eckert, H.; Nilges, T. $\text{Ag}_3\text{SnCuP}_{10}$: [Ag_3Sn] tetrahedra embedded between adamantane-type [P_{10}] cages. *Inorg. Chem.* **2006**, *45*, 5878–5885.
- Lange, S.; Bawohl, M.; Weihrich, R.; Nilges, T. Mineralization routes to polyphosphides: Cu_2P_{20} and $\text{Cu}_5\text{InP}_{16}$. *Angew. Chem. Int. Ed.* **2008**, *47*, 5654–5657.
- Dewalsky, M.V.; Jeitschko, W.; Wortmann, U. The metallic polyphosphide titanium nickel phosphide (Ti_2NiP_5). *Chem. Mater.* **1991**, *3*, 316–319.
- Eisenmann, B.; Rößler, U. Ein Erdalkalimetallpolyphosphid ungewöhnlicher Zusammensetzung: Die Kristallstruktur von Ba_5P_9 . *Z. Anorg. Allg. Chem.* **2003**, *629*, 459–462.
- Chen, X.; Zhu, L.; Yamanaka, S. High-pressure synthesis and structural characterization of three new polyphosphides, $\alpha\text{-SrP}_3$, BaP_8 , and LaP_5 . *J. Solid State Chem.* **2003**, *173*, 449–455.
- Eschen, M.; Jeitschko, W. Au_2PbP_2 , Au_2TlP_2 , and Au_2HgP_2 : Ternary gold polyphosphides with lead, thallium, and mercury in the oxidation state zero. *J. Solid State Chem.* **2002**, *165*, 238–246.
- Kovnir, K.; Stockert, U.; Budnyk, S.; Prots, Y.; Baitinger, M.; Paschen, S.; Shevelkov, A.V.; Grin, Y. Introducing a magnetic guest to a tetrel-free clathrate: Synthesis, structure, and properties of $\text{Eu}_x\text{Ba}_{8-x}\text{Cu}_{16}\text{P}_{30}$ ($0 \leq x \leq 1.5$). *Inorg. Chem.* **2011**, *50*, 10387–10396.
- Fulmer, J.; Kaseman, D.C.; Dolyniuk, J.; Lee, K.; Sen, S.; Kovnir, K. BaAu_2P_4 : Layered Zintl Polyphosphide with Infinite $\frac{1}{\infty}(\text{P}^-)$ Chains. *Inorg. Chem.* **2013**, *52*, 7061–7067.
- Kraus, F.; Korber, N. The Chemical Bond in Polyphosphides: Crystal Structures, the Electron Localization Function, and a New View of Aromaticity in P_4^{2-} and P_5^- . *Chem. A Eur. J.* **2005**, *11*, 5945–5959.
- He, H.; Tyson, C.; Bobev, S. New compounds with $[\text{As}_7]^{3-}$ clusters: Synthesis and crystal structures of the Zintl phases Cs_2NaAs_7 , $\text{Cs}_4\text{ZnAs}_{14}$ and $\text{Cs}_4\text{CdAs}_{14}$. *Crystals* **2011**, *1*, 87–98.
- Knapp, C.M.; Large, J.S.; Rees, N.H.; Goicoechea, J.M. A versatile salt-metathesis route to heteroatomic clusters derived from phosphorus and arsenic Zintl anions. *Dalton Trans.* **2011**, *40*, 735–745.
- Hirschle, C.; Röhr, C. Darstellung und Kristallstruktur der Bekannten Zintl-Phasen Cs_3Sb_7 und Cs_4Sb_2 . *Z. Anorg. Allg. Chem.* **2000**, *626*, 1992–1998.
- Kauzlarich, S.M. *Chemistry, Structure, and Bonding of Zintl Phases and Ion*; John Wiley and Sons Ltd.: New York, NY, USA, 1996.
- Miller, G.J.; Schmidt, M.W.; Wang, F.; You, T.S. Quantitative advances in the Zintl-Klemm formalism. *Struct. Bond.* **2011**, *139*, 1–55.
- Von Schnering, H.G.; Menge, G., Dibariumheptaphosphidchlorid $\text{Ba}_2\text{P}_7\text{Cl}$, eine Verbindung mit dem polycyclischen Anion P_7^{3-} . *Z. Anorg. Allg. Chem.* **1981**, *481*, 33–40.
- Becke, A.D.; Edgecombe, K.E. A simple measure of electron localization in atomic and molecular systems. *J. Chem. Phys.* **1990**, *92*, 5397–5403.

23. Savin, A.; Jepsen, O.; Flad, J.; Anderson, O.K.; Preuß, H.; von Schnering, H.G. Electron localization in solid-state structures of the elements: The diamond structure. *Angew. Chem. Int. Ed.* **1992**, *31*, 187–188.
24. Savin, A.; Nesper, R.; Wengert, S.; Fässler, T.F. ELF: The electron localization function. *Angew. Chem. Int. Ed.* **1997**, *36*, 1808–1832.
25. Kovnir, K.; Kolen'ko, Y.V.; Baranov, A.I.; Neira, I.S.; Sobolev, A.V.; Yoshimura, M.; Presniakov, I.A.; Shevelkov, A.V. Sn₄As₃ revisited: Solvothermal synthesis and crystal and electronic structure. *J. Solid State Chem.* **2009**, *182*, 630–639.
26. Morales, A.; Mora, E.; Pal, U. Use of diffuse reflectance spectroscopy for optical characterization of un-supported nanostructures. *Rev. Mex. Fis. S.* **2007**, *53*, 18–22.
27. Nobbs, J.H. Kubelka—Munk theory and the prediction of reflectance. *Rev. Prog. Color. Relat. Top.* **1985**, *15*, 66–75.
28. SMART and SAINT. Bruker AXS Inc.: Madison, WI, USA, 2007.
29. Sheldrick, G. A short history of SHELX. *Acta Crystallogr. A* **2008**, *64*, 112–122.
30. Jepsen, O.; Burkhardt, A.; Andersen, O.K. *The Program TB-LMTO-ASA*, Version 4.7; Max-Planck-Institut für Festkörperforschung: Stuttgart, Germany, 1999.
31. Barth, U.V.; Hedin, L. A local exchange-correlation potential for the spin polarized case. *J. Phys. C Solid State Phys.* **1972**, *5*, doi:10.1088/0022-3719/5/13/012.
32. Sandia National Labs, Kitware Inc., Los Alamos National Labs (USA). Paraview: Parallel visualization application, version 3.8.1 64 bit. Available online: <http://paraview.org>.
33. Baranov, A.I. *Visualization Plug-in for ParaView*, Version 3.4.11; Springer: Dresden, Germany, 2012.

© 2013 by the authors; licensee MDPI, Basel, Switzerland. This article is an open access article distributed under the terms and conditions of the Creative Commons Attribution license (<http://creativecommons.org/licenses/by/3.0/>).